

Experimental Single-Impulse Magnetic Focusing of Launched Cold Atoms

David A Smith[†], Aidan S Arnold[‡], Matthew J Pritchard[†] and Ifan G Hughes[†]

[†] Department of Physics, Rochester Building, University of Durham, South Road, Durham, DH1 3LE, UK

[‡] SUPA, Department of Physics, University of Strathclyde, Glasgow, G4 0NG, UK

E-mail: i.g.hughes@durham.ac.uk

Abstract. Three-dimensional magnetic focusing of cold atoms with a single magnetic impulse has been observed for the first time. We load 7×10^7 ^{85}Rb atoms into a magneto-optical trap, precool the atoms with optical molasses, then use moving molasses to launch them vertically through 20.5 cm to the apex of flight. In transit the atoms are optically pumped, prior to the single magnetic lens impulse that occurs 16.5 cm above the MOT. Fluorescence images at the apex of flight characterise the widths of the focussed cloud. Results were obtained for four different configurations of the baseball lens, which tuned the relationship between the axial and radial frequencies of the lens. Compact focused clouds were seen for all four configurations.

PACS numbers: 03.75.Be, 32.80.Pj, 39.25.+k

1. Introduction

Laser cooled atoms [1] are now extensively used in a range of experiments spanning fundamental physics and technological applications. As the kinetic energy of ultracold atoms is many orders of magnitude lower than conventional atomic beams, relatively modest electromagnetic forces are now routinely used to gain complete control over the external degrees of freedom of atomic motion. One technique of altering atomic trajectories utilises the Zeeman interaction between an inhomogeneous magnetic field and the magnetic dipole moment of an atom. This Stern-Gerlach force can be used to deflect, reflect and focus paramagnetic cold atoms [2].

Focused cold atoms, obtained using lenses or curved mirrors, are ideal for applications like atom lithography [3] or loading miniature magnetic guides [4] and atom chips [5]. Atom mirrors reverse the velocity component perpendicular to the mirror surface and maintain the component parallel to the surface. In contrast, an atom lens modifies both the transverse and longitudinal velocity components. To date, the Stern-Gerlach force has been used to realise flat [6] and curved [7] permanent atomic mirrors, and pulsed mirrors for both cold (thermal) [8] and Bose condensed atoms [9]. Pulsed magnetic focusing of cold atoms in 3D was first demonstrated by Cornell *et al.* [10] using the alternate-gradient technique. The group of Gorceix

also performed an experimental and theoretical study of magnetic alternate-gradient imaging of cold atoms [11].

We describe the first experiment to focus fully a launched cloud of cold atoms in 3D with a single magnetic lens impulse. In comparison to an unfocused cloud, the density of the cloud can be significantly increased after magnetic focusing. The remainder of the paper is organised as follows: Section 2 gives an overview of atomic focusing; Section 3 outlines the theory and construction of the baseball lens; Section 4 discusses the experimental details; in Section 5 the results are presented; and in Section 6 the results are analysed and conclusions are drawn.

2. An overview of the theory of atom focusing

Consider an atom which starts at the origin and moves along the x -direction with velocity v_x . In order to return the particle to the origin at time T , a single impulse must be applied after a time λT ($0 < \lambda < 1$) at position $x = \lambda T v_x$ changing the atomic velocity to $v_x' = -\frac{v_x \lambda}{1-\lambda} = -\frac{x}{(1-\lambda)T}$. For all velocities, the impulse needed is proportional to the displacement of the atom when it is applied, i.e. a harmonic potential is required. For an atom starting originally at x_0 , a similar analysis shows that the final position is $-x_0(1-\lambda)/\lambda$. Thus, for an ensemble of atoms with a given initial distribution of x_0 values, the spread in final position is independent of the velocity, i.e. a one-to-one image is formed with magnification $(1-\lambda)/\lambda$, exactly analogous to the familiar result of (object distance)/(image distance) in ray optics.

The 1D parabolic lens analysis above assumed an instantaneous impulse; however, extending the analysis to 3D and a finite-duration impulse is straightforward, and is often done in the $ABCD$ -matrix formulation [11, 12, 13]. A finite-duration impulse from a parabolic-potential lens yields a one-to-one image with no dependence on velocity - we term this an aberration-free image. Aberrations arise as a consequence of the departure of the lens potential from being parabolic.

An atom in a magnetic field of magnitude B experiences a magnetic dipole interaction energy of $U = m_F g_F \mu_B B$, where g_F is the Landé g-factor, m_F is the magnetic hyperfine level and μ_B is the Bohr magneton. For a magnetic lens, a constant field (a bias) does not influence the atomic trajectories, a field gradient gives atoms a uniform velocity kick, and a field curvature is used for focusing. The lens angular frequency, ω , along any particular direction for an atom of mass m is given by $\omega^2 = m_F g_F \mu_B B_2 / m$, where B_2 is the field curvature along the corresponding direction. The approximate lens impulse duration, τ , applied at a relative time λT is given by $\omega^2 T \tau = (\lambda(1-\lambda))^{-1}$.

As it is impossible to create a static magnetic field maximum [14], there is only one strategy for producing a focused cloud with a single magnetic impulse - one uses atoms in weak-field-seeking-states, and a lens potential with a minimum at the centre and positive curvature along all three Cartesian axes. This is essentially the requirement for a magnetic trap, for which many designs exist. A magnetic trap/lens also requires a non-zero minimum field, to avoid spin-flip losses [15]. In [12] we analysed the aberrations expected from different magnetic lenses and concluded that a baseball lens would be ideal for achieving single-impulse three-dimensional focusing.

3. The Baseball Lens

The baseball lens is a variant of the Ioffe-Pritchard trap. Ioffe-Pritchard (IP) traps are used extensively for atom trapping and are similar to the Ioffe configuration utilised in plasma confinement [16]. Figure 1(a) shows the geometry. The baseball lens has two components: a nine-turn baseball coil carrying a current I' , and a pair of two-turn circular bias coils which carry the same current I in the same sense. The baseball coil consists of eight straight current-carrying segments of length $w = 10$ cm along x, y , and $\ell = 10$ cm along z . The bias coils have radius $a = 5$ cm and are separated by $s = 5$ cm. The coils were constructed from enamel-coated 3 mm-diameter cylindrical copper wire fixed together with Araldite 2011 epoxy. Further details of the lens construction can be obtained in [17]. The ratio of the axial and radial magnetic curvatures can be tuned via the current ratio I/I' . The bias field is needed because it is impossible to realise a 3D isotropic lens with a baseball coil alone.

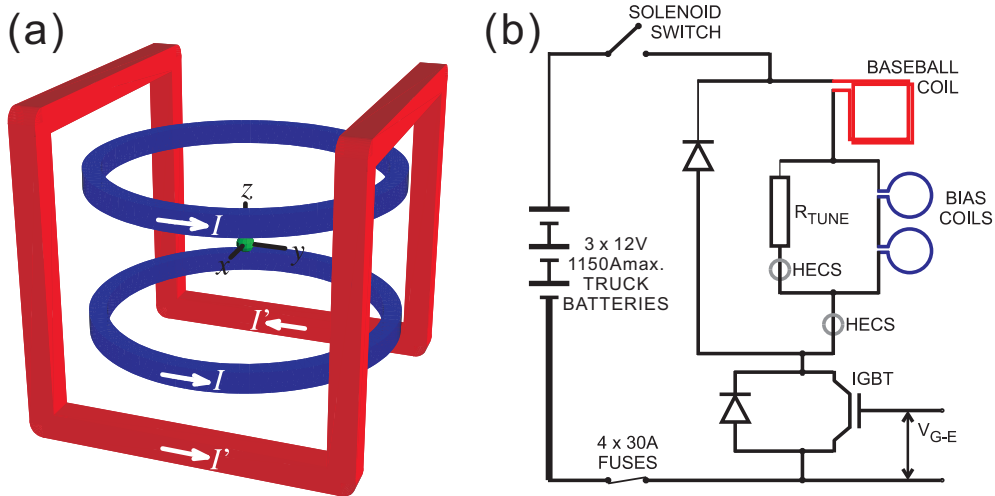


Figure 1. Image (a) shows the baseball lens geometry. The baseball coil is made from 8 straight current-carrying segments; a pair of circular coils provides a bias field. Image (b) is the baseball lens circuit. The current pulse passes through the baseball coil and then the bias coils in parallel with a tuning resistor R_{TUNE} , which is used to control the fraction of baseball current running through the bias coils.

Four configurations of the baseball lens were used in this experiment, i.e. four ratios between the axial and radial curvatures. This was achieved using a tuning resistor R_{TUNE} to regulate the percentage of the total current that passed through the bias coils. The circuit is depicted in Figure 1(b). A Mitsubishi CM1400DU-24NF integrated gate bipolar transistor (IGBT) was used to control the current pulse. To prevent the truck batteries being short-circuited, if the IGBT were to blow open, a 120 A fuse and 12 V solenoid switch were added as automatic and manual safety measures, respectively. The reverse-biased protection diode across the IGBT is inherent within the IGBT module. The reverse-biased Schottky diode (240NQ045) in parallel with the load prevents oscillatory currents in the lens after switch-off. The total current through the baseball coil and the current through the tuning resistor

R_{TUNE} were measured using two Honeywell CSNK591 Hall effect current sensors (HECS in Figure 1(b)). The baseball and bias coils have resistances of 18 m Ω and 3 m Ω , with impedances of 32 μH and 2 μH , respectively. The turn on(off) time for the current is ~ 2 ms.

The third-order expansion of the magnetic field of a baseball lens is [12]

$$\begin{aligned}
 B = B_0 + B'_0 + & \left(\frac{(B'_1)^2}{2(B_0 + B'_0)} - \frac{B'_2 + B_2}{4} \right) (x^2 + y^2) \\
 & + \left(\frac{B'_2 + B_2}{2} \right) z^2 + \left(B'_3 + \frac{B'_1(B'_2 + B_2)}{2(B'_0 + B_0)} \right) (y^2 - x^2) z.
 \end{aligned} \quad (1)$$

Here, B_0 and B_2 are the bias field and field curvature, respectively, originating from the bias coils. B'_0 , B'_1 and B'_2 are the bias field, gradient and curvature, respectively, originating from the baseball coil. Theoretical expressions for these quantities in terms of the currents and dimensions of the baseball and bias coils can be found in [12].

The baseball lens was designed to run with hundreds of Amps for tens of milliseconds; consequently, they were not water-cooled. However, a longer time is needed to measure the field they produce, and hence they were characterised with a 10 A test current. The magnetic field was measured using a Gauss meter with a 1.8 mm diameter circular active area (Bell HTG4-0608) mounted on a translation stage. Table 1 encapsulates the results of these measurements and compares them to the expected values. The measured and theoretical values are in excellent agreement.

Baseball	Measured	Theory	Bias	Measured	Theory	Units
B'_0	0.415(4)	0.42(2)	B_0	0.3596(2)	0.37(2)	G A $^{-1}$
B'_{1x}	14.9(1)	16.6(7)	–	–	–	G m $^{-1}$ A $^{-1}$
B'_{1y}	15.5(2)	16.6(7)	–	–	–	G m $^{-1}$ A $^{-1}$
B_2	260(20)	280(10)	B_2	-25(7)	0 ± 24	G m $^{-2}$ A $^{-1}$

Table 1. Experimental and predicted expansion coefficients for the baseball lens.

4. Experimental Setup

A custom-made stainless steel vacuum chamber was designed for the experiment. The chamber had 12 ports, composed of two intersecting 6-way crosses. One cross had two sets of orthogonal ports in the horizontal plane, and one vertical pair. The other cross had 3 mutually orthogonal axes, symmetrically disposed about the vertical (at an angle $\cos^{-1}(1/\sqrt{3})$), along which the MOT beams propagated. The advantage of this setup is that only two laser frequencies are required to achieve vertical moving molasses. The chamber was pumped with a magnetically-shielded 40 L/s ion pump and the background pressure was 9×10^{-11} Torr. The centre of a square-cross-section glass cell was located approximately 20.5 cm above the MOT to enable the focused atoms to be observed. Three pairs of mutually orthogonal magnetic field coils were used to cancel ambient magnetic fields in the chamber.

A 7×10^7 ^{85}Rb atom MOT was achieved using 6 independent circularly-polarised beams, each of 10 mm ($1/e^2$) radius and power $P = 3$ mW, red-detuned 11 MHz from the ^{85}Rb $5S_{1/2} F = 3 \rightarrow 5P_{3/2} F' = 4$ transition. Approximately 5 mW of repumping

light was shared amongst the 6 MOT beams. The trapping and repumping beams were produced by two separate grating-stabilized, external-cavity diode lasers locked using polarisation spectroscopy [18, 19] with hyperfine pumping/saturated absorption spectroscopy as a frequency reference [20, 21]. Rb vapour was provided by a SAES Rb dispenser. The MOT magnetic quadrupole field had an axial gradient of 15 G/cm.

After collection in the MOT, the atoms underwent a 10 ms 28 MHz-red-detuned optical molasses stage with 25% trap laser intensity, which gave a temperature of (25 ± 2) μ K. A final frequency difference of $\delta\nu = 1.48$ MHz between the upwards and downwards propagating laser beams then launched the atoms vertically in moving molasses at a speed of 2.0 m/s. The frequency ramp of $\delta\nu$ took 3 ms and the final value was held for a further 1 ms. These values were optimised by studying images of the launched cloud up to 20 ms after the launch process. From a mean of five measurements, the initial cloud standard deviations were discerned to be $\sigma_x = 1.01 \pm 0.01$ mm and $\sigma_z = 0.97 \pm 0.01$ mm. After launch, the atoms were optically pumped into the weak-field-seeking $5s^2S_{1/2}|F = 3, M_F = 3\rangle$ state using a 300 mG vertical magnetic field and a 50 μ s pulse of 350 μ W retro-reflected, vertically-propagating, circularly-polarised light resonant with the $^{85}\text{Rb } 5S_{1/2} F = 3 \rightarrow 5P_{3/2} F' = 4$ transition. A sufficient amount of repumping light resonant with the $^{85}\text{Rb } 5S_{1/2} F = 2 \rightarrow 5P_{3/2} F' = 3$ transition was present to prevent atoms from remaining in undesired states.

Fluorescence images of the launched clouds were taken at the apex of flight (204 ms after launch) using a 2 ms duration 6 mW retro-reflected, vertically-propagating, imaging beam resonant with the $^{85}\text{Rb } 5S_{1/2} F = 3 \rightarrow 5P_{3/2} F' = 4$ transition. We were careful to ensure that the imaging pulse did not blur or displace the image of the cloud by virtue of the radiation pressure exerted on the atoms. The centre of the baseball lens was located 16.5 ± 0.2 cm above the MOT. The unfocused cloud came to rest in (approximately) the centre of the image. For each pulsed magnetic lens duration, τ , the lens turn-on time was adjusted to centre the focused cloud in the image, which was taken 204 ms after launch. The area seen in the image was $(x=18.1 \text{ mm}) \times (z=25.8 \text{ mm})$.

5. Results and Analysis

Four different lens configurations were realised, using different values of R_{TUNE} to control the relative current in the bias coil and thus the radial:axial lens frequency ratio. The parameters of these lens configurations (labelled ‘1,’ ‘2,’ ‘3,’ ‘4’) are shown in Table 2.

Lens Config.	I' (A)	I (A)	ω_x (rad s $^{-1}$)	ω_z (rad s $^{-1}$)
1	832 ± 4	832 ± 4	30 ± 1	38 ± 2
2	872 ± 4	446 ± 3	38 ± 1	39 ± 1
3	898 ± 4	304 ± 2	41 ± 2	39 ± 2
4	947 ± 5	0	50 ± 2	40 ± 2

Table 2. Parameters for lens configurations. The slight variation of ω_z is due to the non-zero value of B_2 for the bias coils.

Figure 2 shows a sequence of images obtained with increasing baseball pulse duration, τ , using lens configuration 1. A background image with no atoms launched

is shown in (a). In (b) a cloud of atoms was launched but not focused. For the launch temperature, it is expected that the width of the unfocused Gaussian cloud is significantly larger than the area imaged onto the CCD chip. Images (c) - (i) show the variation of the focused cloud as a function of τ . The cloud comes to a focus in the x -direction between 16 and 20 ms, and in the z -direction between 28 and 32 ms. Three-dimensional focusing of a launched cloud with a single impulse from a baseball lens is clearly seen.

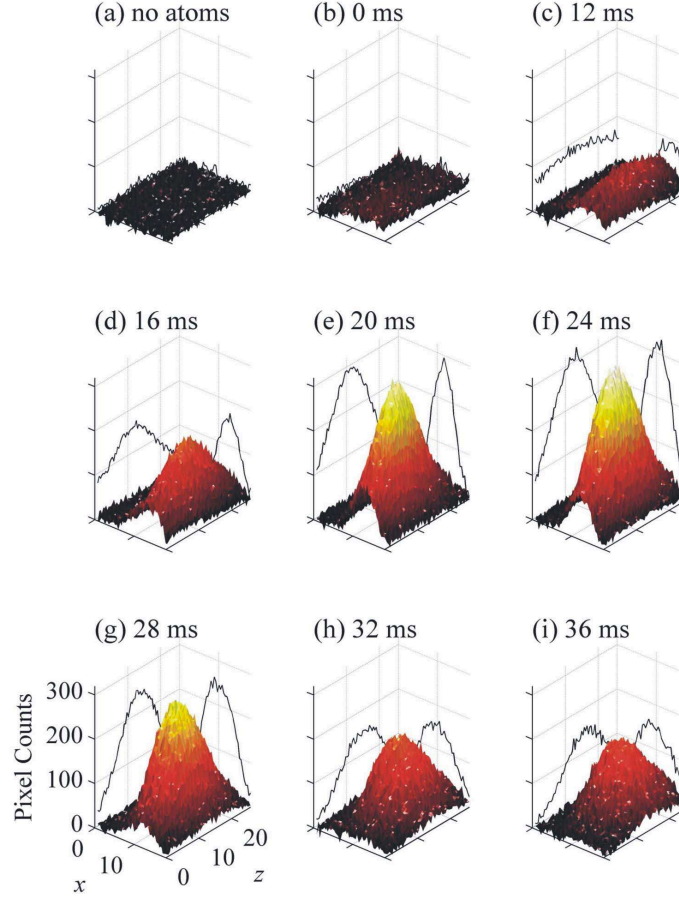


Figure 2. A sequence of images for increasing baseball lens duration, τ , using lens configuration 1. (a) Image taken, but no atoms launched; (b) typical image of launched atoms, without lensing ($\tau = 0$); (c) - (i) τ increases from 12 ms to 36 ms in 4 ms steps. The x and z axes are in mm.

Figure 3 shows the cloud sizes (standard deviations) along the x - and z -directions for different durations of the impulse, τ , for all four lens configurations. Three-dimensional magnetic focusing with a single magnetic impulse has been observed for all four configurations, most notably using lens configuration 1. The radial frequency of a Ioffe-Pritchard trap increases with decreasing bias field. This is reflected in the data, because as we change from lens configuration 1 to lens configuration 4, the radial

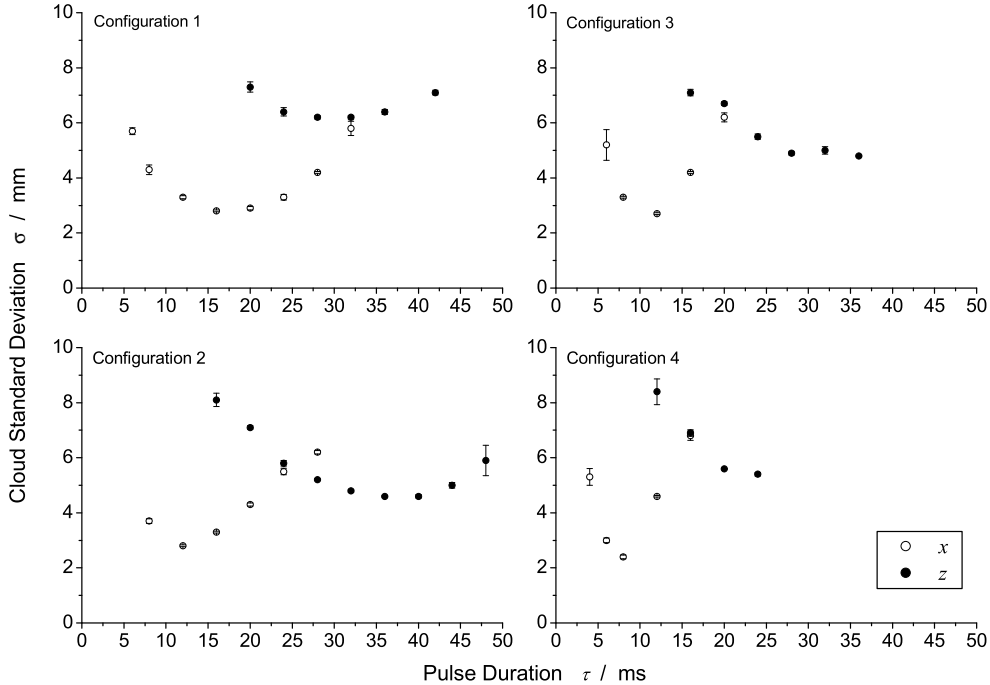


Figure 3. Plots of the cloud sizes along the x - and z -directions, as functions of pulse duration, τ , for the four lens configurations.

angular frequency increases and the pulse duration required to achieve the minimum x -focus decreases. The minimum measured value of the standard deviation in the x -direction of a focused cloud was 2.43 ± 0.07 mm, using lens configuration 4 with a pulse duration $\tau = 8$ ms. The minimum measured value of the standard deviation in the z -direction of a focused cloud was 4.57 ± 0.03 mm, using lens configuration 3 and a pulse duration of $\tau = 36$ ms. For all four lens configurations, the minimum radial cloud width is smaller than the minimum axial width.

5.1. Analysis of cloud size for different lens configurations

Two methods of predicting the expected cloud size were employed. First, an $ABCD$ -matrix analysis was carried out, characterising the lens as being perfectly parabolic with a finite-duration impulse. This analysis is easy to perform, but as we pointed out in [12], the limit of the validity of the assumptions underlying this method are unlikely to extend to a realistic experiment. The second method is a brute-force numerical simulation of the trajectories of many atoms subject to the forces of gravity and a pulsed Stern-Gerlach force. In this model, the magnetic field was calculated by taking the baseball coil to be constructed from eight equal-length, straight, infinitesimally-thin conductors, which ignored the finite extent of the conductors in the 3×3 array of the real lens. The bias coils were modelled as single current loops, rather than the 2-turn coils in the experimental lens. Further details of the numerical simulation can be found in [12]. Figure 4 compares the experimentally obtained cloud size along the x -direction with the matrix and numerical simulations.

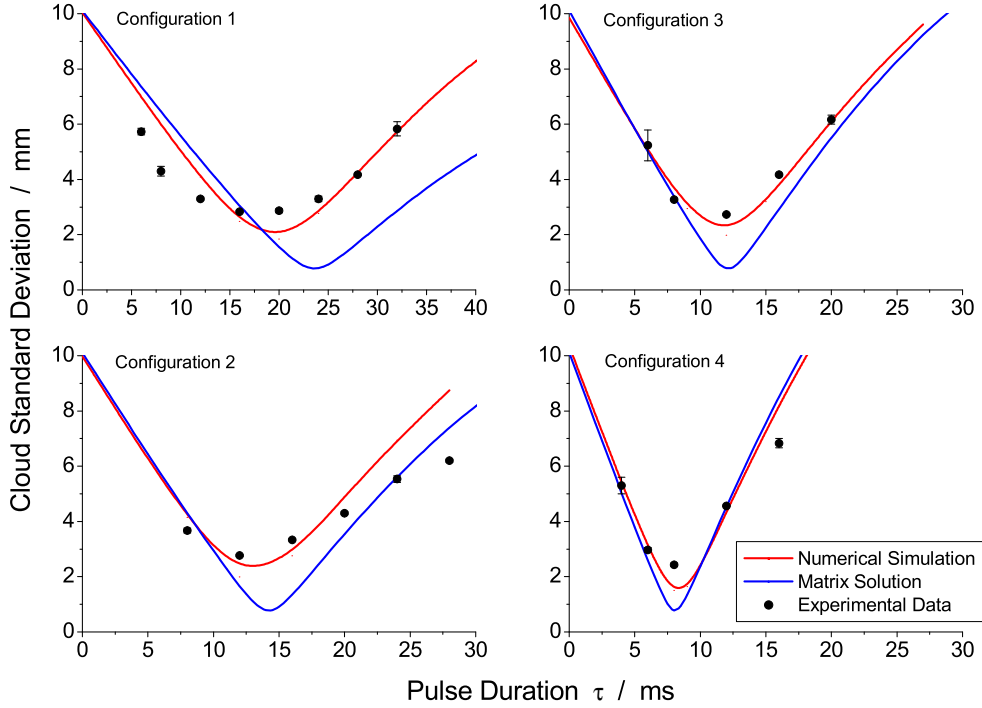


Figure 4. Plots of the cloud size along the x -direction as a function of the pulse duration, τ , and comparison with an $ABCD$ -matrix analysis and a numerical simulation.

For the matrix analysis, the initial cloud position and standard deviation are required as input - these were deduced from experimental measurements. It is then possible to obtain analytic predictions for the cloud-size dependence on τ as a function of ω_x . A least-squares comparison of the data and matrix prediction were made, and the results are summarised in table 3. The values for ω_x deduced from the experimental data are seen to be in good agreement with those predicted from knowledge of the geometry and currents passed through the baseball lens.

Lens	Predicted ω_x (rad s ⁻¹)	Fitted ω_x (rad s ⁻¹)
1	30	33
2	38	39
3	41	44
4	50	50

Table 3. Predicted and fitted values of ω_x , the radial angular frequency.

Although the radial frequencies deduced are in good agreement with the expected values, the matrix analysis consistently predicts minimum cloud sizes which are smaller than those measured experimentally. The numerical analysis is seen to show far better agreement with the minimum cloud size. This confirms the predictions presented in [12] that aberrations arising from terms beyond the ideal parabolic lens

approximation are significant.

A similar analysis was performed for the size of the cloud measured along the z -direction. However, as the data do not show good agreement with either the matrix or numerical simulations we do not present the analysis here. Numerical simulations show that the focusing properties in the z -direction are far more sensitive to slight misalignment of the centre of the cloud with respect to the centre of the lens than for the radial direction.

6. Conclusions

Three-dimensional magnetic focusing of cold atoms with a single-impulse magnetic lens has been observed for the first time. Results were obtained for four different configurations of the baseball lens, which varied the relationship between the axial and radial angular frequencies of the lens. Compact focused clouds were seen for all four configurations. $ABCD$ -matrix analysis of the experimental data for the variation of the focused cloud size was in good agreement for the horizontal (x) direction, but did not account for the behaviour of the focused cloud in the vertical (z) direction. Numerical simulations showed very good agreement with the horizontal cloud size, but were not able to account fully for the behaviour of the cloud size in the direction in which the atom cloud had been launched. The complex issue of the discrepancy between the predictions (both analytical and numerical) for vertical cloud size and the obtained experimental data is an ongoing investigation.

In addition to a study of atom focusing, these results present a method of transferring cold atoms from a MOT to a remote vacuum chamber. This method can be compared to two other magnetic transfer mechanisms. It is possible to load atoms into a magnetic trap in one chamber and magnetically transport the atoms into a remote chamber using either time-dependent currents in an array of static coils [22] or trap coils mounted on a motorised stage [23]. The disadvantage of a scheme with static coils is the large number of coils and power supplies required, and the time-dependent currents. Initial experiments with moving coils used a three-dimensional quadrupole trap, which has a magnetic zero at its centre. For certain applications, a trap with a finite minimum is required, and recently transport of atom packets in a train of Ioffe-Pritchard traps was demonstrated [24]. Using moving coils does, however, place limitations on vacuum chamber design since sufficient space must be allowed for the translation mechanism. The pulsed magnetic lens presented in this work needs, realistically, only space for the lens itself. In contrast to this work, there is no significant increase in cloud size with the two magnetic transport schemes described above; however, in theory a pulsed magnetic lens could result in a bimodal focus with a very tightly focused 3D core of atoms, denser than the initial distribution, as shown in [13]. The combination of pulsed magnetic focusing combined with laser guiding looks promising [25]

In this work, spatial focusing was considered. A possible future extension would be to study velocity focusing, and recently a Ioffe-Pritchard lens was used for this purpose [26]. A wavepacket with a very narrow momentum distribution is ideal for studying quantum tunnelling, and a 1-dimensional narrow momentum distribution could also be useful for other atom optics experiments, such as studying quantum accelerator modes.

Acknowledgments

This work is supported by EPSRC. We thank Charles Adams and Simon Cornish for fruitful discussions. Simon Cox assisted with the construction of the vacuum chamber. Kevin Weatherill designed the external-cavity laser.

References

- [1] Chu S 1998 *Rev. Mod. Phys.* **70** 685; Cohen-Tannoudji C N 1998 *Rev. Mod. Phys.* **70** 707; Phillips W D 1998 *Rev. Mod. Phys.* **70** 721
- [2] Hinds E A and Hughes I G 1999 *J. Phys. D* **32** R119
- [3] Meschede D and Metcalf H 2003 *J. Phys. D* **36** R17
- [4] Müller D *et al.* 1999 *Phys. Rev. Lett.* **83** 5194; Dekker N H *et al.* 2000 *Phys. Rev. Lett.* **84** 1124; Key M *et al.* 2000 *Phys. Rev. Lett.* **84** 1371
- [5] Folman R *et al.* 2002 *Adv. At. Mol. Opt. Phys.* **48** 263; Reichel J 2002 *Applied Physics B* **74** 469
- [6] Roach T M *et al.* 1995 *Phys. Rev. Lett.* **75** 629; Sidorov A I *et al.* 1996 *Quantum Semiclass. Opt.* **8** 713; Lau D C *et al.* 1999 *Eur. Phys. J. D* **5** 193; Sidorov A I *et al.* 2002 *Acta Physica Polonica B* **33** 2137; Lev B *et al.* 2003 *Applied Physics Letters* **83** 395; Mohapatra A K and Unnikrishnan C S 2006 *Europhys. Lett.* **73** 839
- [7] Hughes I G *et al.* 1997 *J. Phys. B: At. Mol. Opt. Phys.* **30** 647; *ibid* **30** 2119; *ibid* **34** 2869; Saba C V *et al.* 1999 *Phys. Rev. Lett.* **82** 468
- [8] Kadio D, Houde O and Pruvost L 2001 *Europhys. Lett.* **54** 417
- [9] Bloch I *et al.* 2001 *Phys. Rev. Lett.* **87** 030401; Arnold A S, MacCormick C and Boshier M G 2002 *Phys. Rev. A* **65** 031601(R); Arnold A S, MacCormick C and Boshier M G 2004 *J. Phys. B* **37** 485; Köhl M *et al.* 2005 *Phys. Rev. A* **72** 063618
- [10] Cornell E A, Monroe C and Wieman C E 1991 *Phys. Rev. Lett.* **67** 2439
- [11] Miossec T, Barbé R, Keller J-C and Gorceix O 2002 *Opt. Commun.* **209** 349
- [12] Pritchard M J, Arnold A S, Smith D A and Hughes I G 2004 *J. Phys. B* **37** 4435
- [13] Arnold A S, Pritchard M J, Smith D A and Hughes I G 2006 *New Journal of Physics* **8** 53
- [14] Earnshaw S 1842 *Trans. Cambridge Philos. Soc.* **7** 97; Wing W H 1984 *Prog. Quant. Electr.* **8** 181
- [15] Petrich W *et al.* 1995 *Phys. Rev. Lett.* **74** 3352
- [16] Gott Y V, Ioffe M S and Tel'kovskii V G 1962 *Nucl. Fusion Suppl.* **3** 1045; Pritchard D E 1983 *Phys. Rev. Lett.* **51** 1336
- [17] Smith D A 2005 PhD. Thesis, University of Durham, UK (unpublished)
- [18] Wieman C and Hänsch T W 1976 *Phys. Rev. Lett.* **36** 1170
- [19] Pearman C P *et al.* 2002 *J. Phys. B* **35** 5141; Harris M L *et al.* 2006 *Phys. Rev. A* **73** 0625509
- [20] MacAdam K B, Steinbach A and Wieman C E 1992 *Am. J. Phys.* **60** 1098
- [21] Smith D A and Hughes I G 2004 *Am. J. Phys.* **72** 631
- [22] Greiner M, Bloch I, Hänsch T W and Esslinger T 2001 *Phys. Rev. A* **63** 031401
- [23] Lewandowski H J *et al.* 2003 *J. Low Temp. Phys.* **132** 309; Goldwin J, Inouye S, Olsen M L, Newman B, DePaola B D and Jin D S 2004 *Phys. Rev. A* **70** 021 601(R); Nakagawa K *et al.* 2005 *Appl. Phys. B* **81** 791-794
- [24] Lahaye T, Reinaudi G, Wang Z, Couvert A and Guéry-Odelin D 2006 *Phys. Rev. A* **74** 033622
- [25] Pritchard M J *et al.* 2006 *New J. Phys.* **8** 309
- [26] Aoki T, Kato T, Tanami Y and Nakamatsu H 2006 *Phys. Rev. A* **73** 063603